encit 2020

ABCM
Associação Brasileira de Engenharia e Ciências Mecânicas

18th Brazilian Congress of Thermal Sciences and Engineering
November 16–20, 2020 (Online)

ENC-2020-0119
ASSESSMENT OF MACH NUMBER EFFECTS ON SECONDARY TONES ARISING IN AIRFOIL FLOWS

Tulio Rodarte Ricciardi
William Roberto Wolf
University of Campinas
tulioricci@fem.unicamp.br, wolf@fem.unicamp.br

Abstract. *Direct numerical simulations are carried out to investigate the flow features responsible for secondary tones in airfoil noise at Reynolds number $Re_c = 5 \times 10^4$. Results show that noise emissions have a main tone with equidistant secondary tones, as discussed in literature. Flow simulations of a NACA 0012 airfoil are conducted for freestream Mach numbers ranging from 0.2 to 0.4 at 3 deg. angle of incidence. Initial findings show that a low-frequency modulation of the vortex dynamics induces phase variation of flow instabilities developed along the airfoil boundary layer. The modulation directly affects the velocity and pressure fluctuations that are scattered at the trailing edge, resulting in acoustic radiation of secondary tones.*

Keywords: *Aeroacoustics, vortex dynamics, frequency modulation*

1. INTRODUCTION

The understanding of trailing-edge noise is an overriding concern for design of noise-efficient aerodynamic shapes including wings and high-lift components, wind turbine and helicopter blades, fans and even car roof racks (Massarotti and Wolf (2018)). For such devices, tonal noise may be an important component of the noise spectrum, especially at moderate Reynolds number flows. At these conditions, vortex shedding due to laminar boundary layer instabilities and blunt trailing edges are identified by Brooks *et al.* (1989) as potential sources of airfoil tonal noise. Wolf *et al.* (2012a, 2013, 2012b) and Ricciardi *et al.* (2019) performed numerical investigations of turbulent flows past different airfoils with blunt trailing edges and showed that tonal noise may appear in far-field acoustic predictions even in the presence of fully turbulent boundary layers.

Several pioneering studies of airfoil aeroacoustics were conducted in the 1970s to examine tonal noise generation. These investigations showed that discrete tones are emitted at specific flow conditions (see Clark (1971); Hersh and Hayden (1971); Longhouse (1977)). Such findings triggered some of the first systematic and detailed studies of airfoil tonal noise (Paterson *et al.* (1973); Tam (1974); Fink (1975); Arbey and Bataille (1983)). Paterson *et al.* (1973) performed noise measurements from symmetric NACA airfoils for a Reynolds number range between 10^5 and 10^6 at various angles of attack; their results showed the existence of multiple tones in a ladder-like structure pattern in terms of frequency and freestream velocity. Furthermore, they found a strong correlation in terms of spanwise surface pressure fluctuations on the airfoils, showing that the flow phenomenon associated with tonal noise generation could be modeled as two-dimensional.

Arbey and Bataille (1983) repeated the experiments from Paterson *et al.* (1973) in an open wind tunnel for three different NACA airfoils and showed that the noise spectrum was composed of a broadband contribution with a main tonal peak plus a set of equidistant secondary tones. They argue that acoustic waves propagate upstream and create a feedback loop, with the separation bubble acting as an amplifier of acoustic disturbances. Later, supporting this model, Desquesnes *et al.* (2007) showed that the main acoustic tone frequency radiated to the far-field was close to that most amplified along the pressure side boundary layer. These authors performed 2D direct numerical simulations (DNS) of flows past a NACA0012 airfoil for Reynolds numbers 1×10^5 and 2×10^5 with angles of attack of 2 and 5 degs. Their results presented multiple tonal peaks consistent with experimental observations from Arbey and Bataille (1983). Following the results of Desquesnes *et al.* (2007), Pröbsting *et al.* (2014) employed particle image velocimetry to investigate the mechanisms associated with tonal noise generation. These authors discussed about an amplitude modulation of velocity fluctuations measured near the trailing edge. de Pando *et al.* (2014) employed both 2D DNS and global stability analysis to study the dynamics of hydrodynamic and acoustic wavepackets driving the feedback loop mechanism. Another recent work that makes the connection between tones and TS waves is presented by Sanjose *et al.* (2019) for a controlled-diffusion airfoil at $Re_c < 5 \times 10^5$. These authors employed a suit of modal analysis techniques to investigate the tonal noise generation problem and found that intermittency plays a significant role in the flow dynamics and noise emission of the airfoil configuration investigated.

It is clear that since the 1970s, great efforts have been carried out to improve the understanding of the airfoil tonal noise phenomenon and we suggest the review paper by Arcondoulis *et al.* (2010) for a general discussion on the topic. As one can see, there are still several open questions and disagreements in literature with respect to trailing edge tonal noise.

The current work presents a numerical study of airfoil tonal noise generation at a moderate Reynolds number flow. We investigate effects of compressibility on both the acoustic signature and flow dynamics, and particular attention is given to the appearance of secondary tones in spectra. The flow configurations are analyzed at 3 deg. AoA for freestream Mach numbers $M_\infty = 0.2$ to 0.4, for a Reynolds number based on the chord of $Re_c = 5 \times 10^4$. In a recent work, Ricciardi *et al.* (2020) showed for $M_\infty = 0.3$ that vortical structures are shed with phase variations due to frequency modulation by the separation bubble on the airfoil surface, resulting in acoustic radiation of secondary tones. Here, we continue this study showing further analyses of compressibility effects on tonal noise generation where secondary tones play an important role.

2. Numerical Methodology

Direct numerical simulations are conducted solving the two-dimensional compressible Navier-Stokes equations in general curvilinear coordinates. Length, velocity components, density and pressure are non-dimensionalized by the airfoil chord, L, freestream speed of sound, a_∞, freestream density, ρ_∞ and $\rho_\infty a_\infty^2$, respectively. For sake of comparison, results in terms of time and frequency are presented non-dimensionalized by freestream velocity as $t = t^* U_\infty / L$ and $St = f^* L / U_\infty$. In these definitions, t^*, f^* and St are time (dimensional), frequency (dimensional) and Strouhal number, respectively.

A staggered grid sixth-order accurate compact scheme (Nagarajan *et al.* (2003)) is employed for the spatial discretization of the governing equations. Away from solid boundaries, a high wavenumber compact filter (Lele (1992)) is applied to control numerical instabilities arising from mesh non-uniformities and interpolation at grid interfaces. The time integration is carried out by the implicit second-order scheme of Beam and Warming (1978) in the near-wall region while a third-order Runge-Kutta scheme is used for time advancement of the equations in flow regions far away from solid boundaries. No-slip adiabatic wall boundary conditions are applied along the solid surfaces and characteristic plus sponge boundary conditions are applied in the far-field locations to minimize wave reflections. The numerical tool has been previously validated for several 2D and 3D simulations of compressible flows involving airfoil sound generation (Wolf *et al.* (2012a, 2013, 2012b); Ricciardi *et al.* (2019)).

3. Results and Discussion

An airfoil immersed in a low Reynolds number flow emits a single tone due to vortex shedding while, for higher Reynolds numbers, airfoil noise is typically broadband due to turbulent boundary layers. At moderate Reynolds numbers, the mechanisms of noise generation are modified by the presence of Tollmien-Schlichting (TS) instabilities developed along the boundary layer. These instabilities have large spanwise coherence being efficient noise sources due to acoustic scattering at the trailing edge. Depending on additional parameters of the flow, multiple secondary tones may appear on the far-field pressure spectrum Desquesnes *et al.* (2007). In this work, the study of secondary tones is conducted by means of spectral analysis of signals, including frequency-domain and time-frequency techniques. The analyses are presented in terms of hydrodynamic quantities, such as velocity in the boundary layer, and pressure fluctuations measured on the acoustic field.

In this section, we present results of 2D direct numerical simulations for moderate Reynolds number flows past a NACA0012 airfoil to understand the effects of compressibility on tonal noise generation. The Reynolds number is set as $Re_c = 5 \times 10^4$ for all cases. A description of the different flows investigated is presented in Table 1 in terms of freestream Mach number (M_∞), mesh configuration (nx, ny), wall-normal spacing (Δn_w) and computational domain size. The latter includes a sponge layer in the far-field to damp the wake and acoustic waves before they reach the farfield boundaries. Table 1 also includes the time step (Δt) and total period of simulation (T) for which data is recorded. For the spectral analysis, time series are acquired at a frequency sampling $f_s \geq 133.3$ and we apply overlap of 67% among the bins using a Hanning window with a frequency resolution of $\Delta f = 0.03$.

Table 1. Description of flow configurations investigated.

$\boldsymbol{M_\infty}$	0.2	0.3			0.4
nx	660	440	660	990	660
ny	600	480	600	600	600
Far-field	32	32	32	24	32
$\boldsymbol{\Delta n_w \times 10^4}$	1	2	1	0.66	1
$\boldsymbol{\Delta t \times 10^4}$	1.25	1.80	1.25	0.75	1.25
T	300	300	300	300	300

The airfoil geometry has an effective chord of 98% from the original NACA0012 profile and a rounded trailing-edge with a radius of 0.4% of the chord length to allow for a smooth O-grid mesh generation. The surface grids have a ratio of approximately 5:3 points on suction relative to pressure side. A detail view of the medium mesh near-field is presented in Fig. 1, where every 4th grid point is shown in both directions.

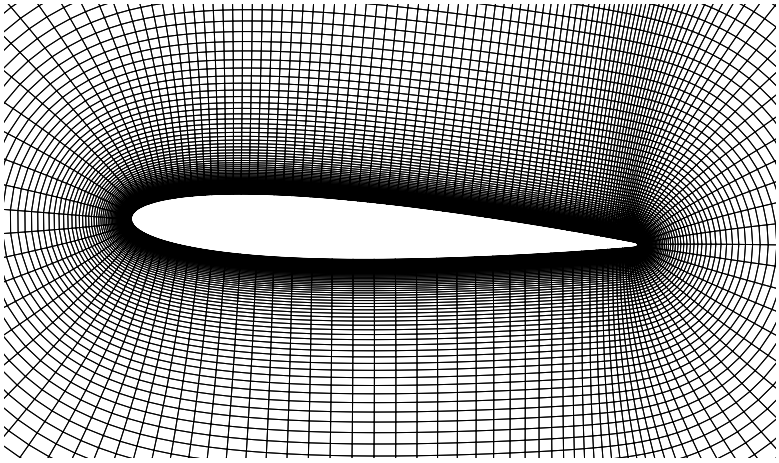

Figure 1. Detail view of grid with N_x = 660, N_y = 600, $\mathbf{\Delta} n_w$ = 0.0001, Δx_{LE} = 0.001 and Δx_{TE} = 0.00016.

Initially, different grid configurations are investigated only for $M_\infty = 0.3$ in order to assess resolution in terms of hydrodynamic properties. Results are presented in Figs. 2 to 6 for mean properties such as velocity profiles along the wall normal direction and wake, besides pressure and friction coefficients. Figure 2 presents the main features of the mean flow in terms of U-velocity contours. Due to geometry asymmetry, the flow first accelerates on the suction side of the airfoil and, then, decelerates, forming a separation bubble and a shear layer. Flow separation occurs at $x/c \approx 0.35$ and the region with reversed flow is highlighted by a line with magenta color. At $x/c \approx 0.82$, the mean flow reattaches to the surface. Data acquisition is performed with a higher sampling frequency at the white circles indicated in the figure.

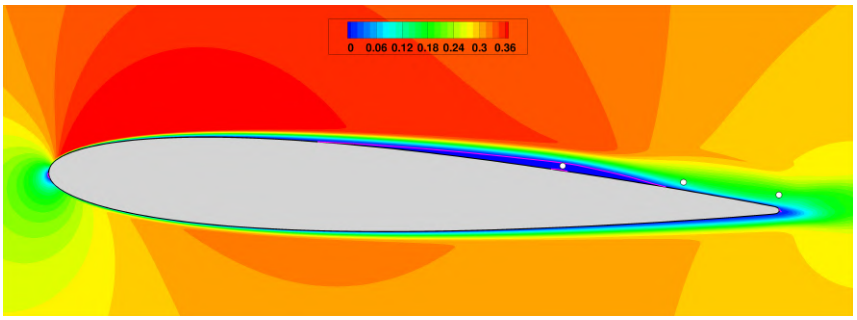

Figure 2. Mean flow contours of u-velocity component for $M_\infty = 0.3$. One should remind that the velocity is non-dimensional by speed of sound.

Figure 3 shows results of boundary layer mean velocity profiles computed in the wall-normal direction for different airfoil chord positions, including both tangential $\langle V_t \rangle$ and normal $\langle V_n \rangle$ components. The latter is shown by the dotted lines while the former is shown by the different styles (continuous, dashed, dash-dotted) as presented in the legend. From the mean velocity profiles, one can observe that, at $x/c = 0.35$, the flow has inflection point and it is on the verge to separate. At $x/c = 0.69$, the flow is separated what indicates that this profile is computed inside the recirculation bubble and, finally, at $x/c = 0.85$, the flow is already reattached.

In terms of velocity in the wake, Fig.4 shows the mean $\langle U \rangle$-velocity component downstream the airfoil for profiles at $x/c = 1.1, 1.2$ and 1.5. These profiles allow a comparison in terms of momentum deficit. All grids provide good comparisons for the measurements just downstream the trailing edge at $x/c = 1.1$. However, the mesh coaserning shows discrepancies that can be visualized in the oscillatory behavior when the velocity recovers from the wake towards the freestream. This may indicate that some flow structures shed from the trailing edge are dissipated by the coarser meshes while the finest grid may still be able to capture.

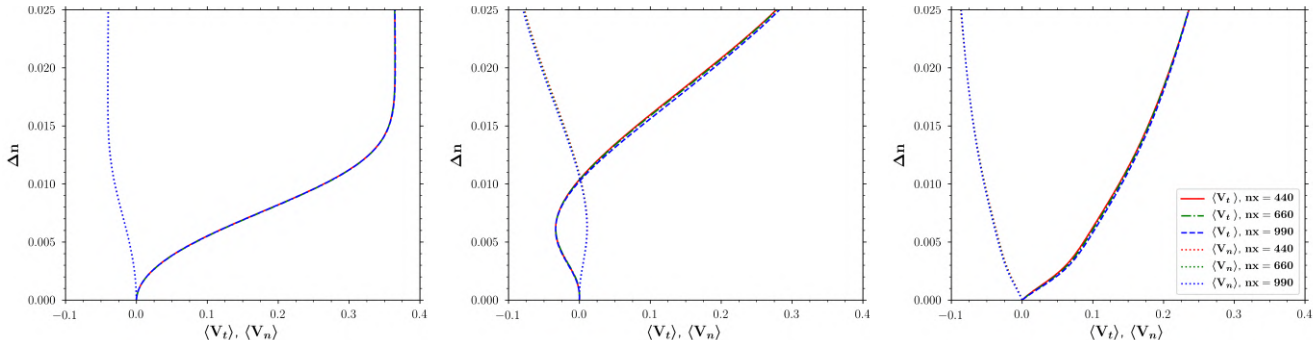

(a) $x = 0.35$. (b) $x = 0.69$. (c) $x = 0.85$.

Figure 3. Mean tangential and normal velocity profile in the boundary layer for different positions.

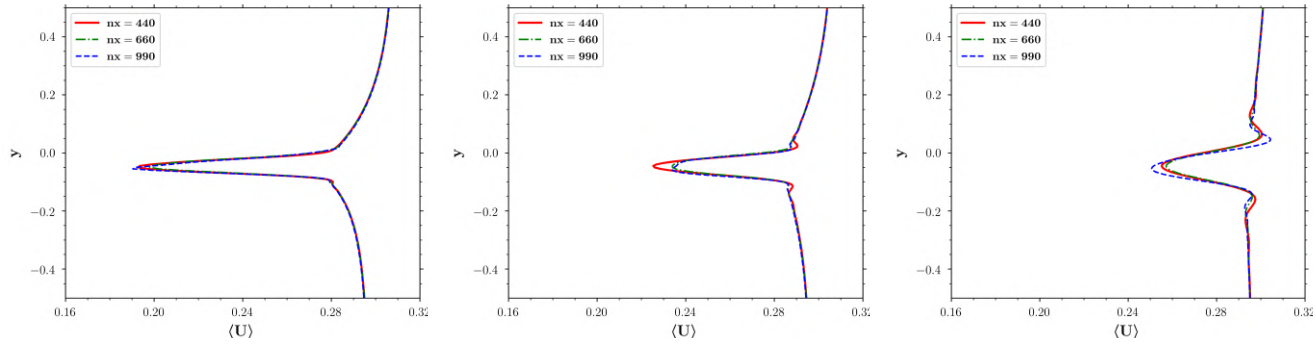

(a) $x = 1.1$. (b) $x = 1.2$. (c) $x = 1.5$.

Figure 4. Mean U velocity profile for several positions along the wake.

Flow fluctuations are analyzed inside the boundary layer in Fig. 5, which presents spectra of u-velocity inside the recirculation bubble at $x = 0.69$, and above the trailing edge, at $x = 0.98$. In these figures, multiple equidistant tones can be observed around a dominant frequency (Arbey and Bataille (1983); Desquesnes *et al.* (2007); Ricciardi *et al.* (2020)). These multiple tones are either the cause or consequence of spectral patterns observed in the flow field such as frequency and amplitude modulation of hydrodynamic structures. Some discrepancies in magnitude are observed among all grids, however, the dominant peak at $St = 2.5$ and its harmonics at 5.0 and 7.5 have a very good agreement. The solutions obtained by the different grids seem to agree with respect to the tone frequencies and magnitude. Hence, the dominant features of the flow seem to be well converged even in spectral quantities.

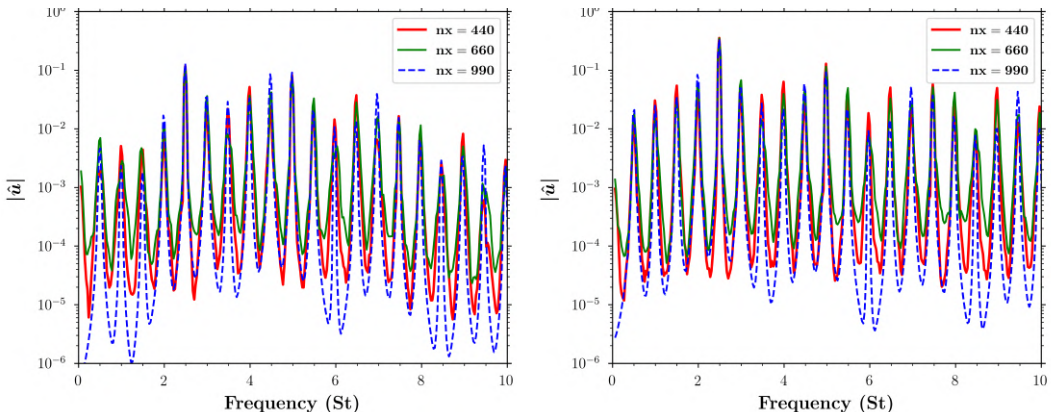

(a) Recirculation bubble $x = 0.69$. (b) Trailing edge $x = 0.98$.

Figure 5. FFT coefficients for $|\hat{u}|$ computed at different chord locations.

Results in terms of steady skin friction and pressure coefficient distributions are presented in Fig. 6 below. Differences among the 3 grid resolutions are minimal and can only be noticed in the region between $0.7 < x < 0.98$, downstream to the reattachment point. One should notice that the separation bubble is given by the negative values of C_f up to $x/c \approx 0.67$. Downstream this position, the negative values of C_f are even more pronounced but that region is related to the strong vortical structures shed by the shear layer and that, on average, appear as separated flow region.

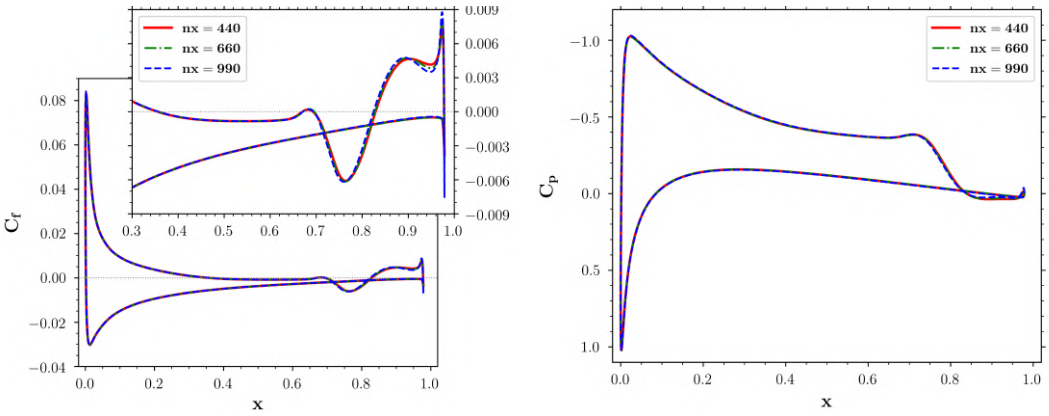

(a) C_f. (b) C_p.

Figure 6. Surface distribution of skin friction and pressure coefficients.

Considering that the grid with medium resolution provides accurate converged results, the effects of compressibility are investigated changing the freestream velocity in the simulations. Hence, from now on, velocities will be presented normalized by the respective M_∞ for a comparison of the different setups. Results in terms of velocity profiles are shown in Fig. 7 for both tangential $\langle V_t \rangle$ and normal $\langle V_n \rangle$ components.For the higher Mach number, both boundary layer and separation bubble are thicker, which can be attributed to the higher temperature that increases viscosity of the flow, while the opposite is also true. In terms of wake velocity, Fig. 8 presents similar trends, i.e., the solution for $M_\infty = 0.4$ presents a larger velocity deficit.

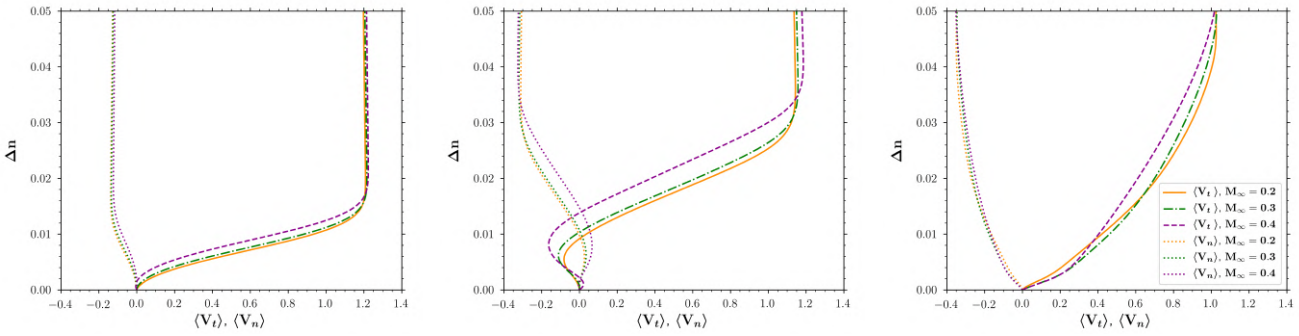

(a) $x/c = 0.35$. (b) $x/c = 0.69$. (c) $x/c = 0.85$.

Figure 7. Mean tangential and normal velocity profiles in the boundary layer for different chord positions.

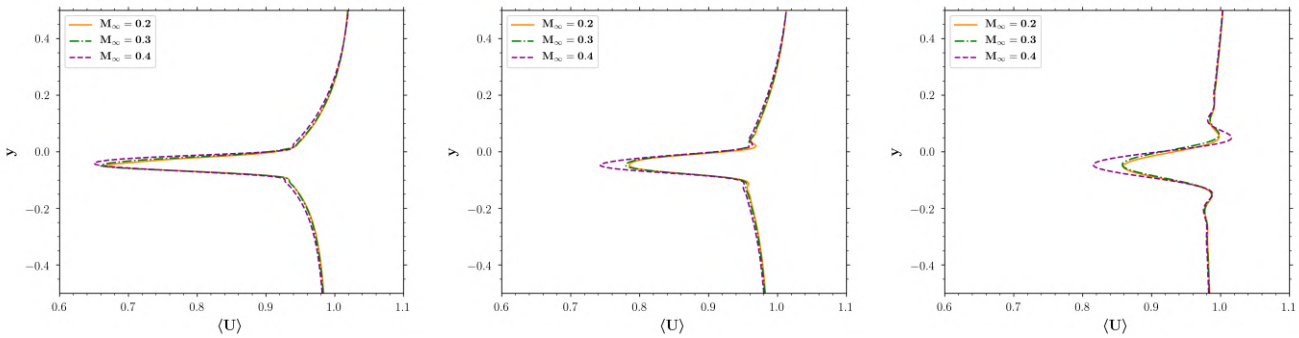

(a) $x/c = 1.1$. (b) $x/c = 1.2$. (c) $x/c = 1.5$.

Figure 8. Mean U velocity profiles for several positions along the wake.

The spectral analysis of the hydrodynamic field is performed for a probe at $x/c = 0.69$, inside the recirculation bubble, and at $x/c = 0.98$, aligned with the trailing edge. When the Strouhal number is non-dimensionalized by the boundary layer thickness at $x/c = 0.69$, Fig. 9 shows that it is possible to see an alignment of the tones, plotted as a function of St_δ. The thickness δ is given by the normal distance from the wall up to the point where the tangential velocity is 99% of M_∞. This normalization is justified due to different thicknesses of the boundary layers, what leads to different

length and frequency scales of vortex shedding. Figure 9 also shows that the main tones change frequency depending on the freestream Mach number and that higher Mach numbers excite higher non-dimensional frequencies based on St_δ. The main tone amplitudes also seem to increase with Mach number but that observation can be related to specific probe locations.

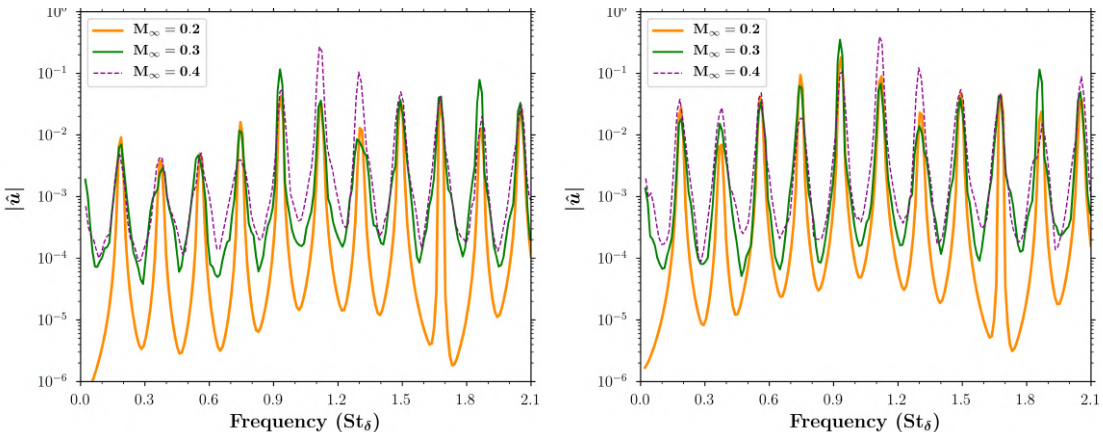

(a) Recirculation bubble, $x/c = 0.69$. (b) Trailing edge, $x/c = 0.98$.

Figure 9. Fourier coefficients for $|\hat{u}|$ computed at different chord positions.

Figure 10(a) shows how the skin friction is modified by the different Mach number flows: the higher the Mach number, the higher variation in friction coefficient on the wall. Such variations are observed mainly along the separation bubble and downstream, where the vortical structures are shed by the shear layer. Similar variations can also be seen in the pressure coefficient plots of Fig. 10(b). The behavior of the skin friction coefficient for $M_\infty = 0.3$ is illustrated in Fig. 11 by snapshots of the flow field at different instants. In these pictures, the mean $< U >$-velocity flow field is presented in contours, while the region of negative velocity is limited by the magenta line. To highlight the vortices, z-vorticity is displayed in black and white colors (levels of -20 and $+20$ respectively). The white circles are probe locations and they are placed at $x/c = 0.69, 0.85$ and 0.98. It is possible to see that the vortices (black lines, with negative z-vorticity) detach from the shear layer in the region between $0.62 \lesssim x/c \lesssim 0.70$, where the friction coefficient starts to show changes in the flow direction, with a rapid reattachment of the mean flow. Then, from $0.70 \lesssim x/c \lesssim 0.80$, the close proximity of the vortices leads to a vortex-merging process, resulting in strong oscillations in skin friction. Also, during the shedding and merging of structures, an eruption process in the boundary layer is present where the flow close to the wall is sheared and ejected towards the mean flow (white spots, with positive z-vorticity).

In the region where the flow is recirculating, it is possible to see a plateau in Fig. 10(b) in terms of pressure coefficient. Downstream the airfoil, for the same position where there is the vortex pairing, a sudden drop in pressure leads to the hump observed for $x/c \approx 0.7$. Another important remark in terms of pressure is that the higher Mach number increases Cp on the suction side. This may be related to the thicker boundary layer that leads to a flow acceleration and, hence, lower pressure. In this case, the airfoil would be perceived by the flow as a thicker profile.

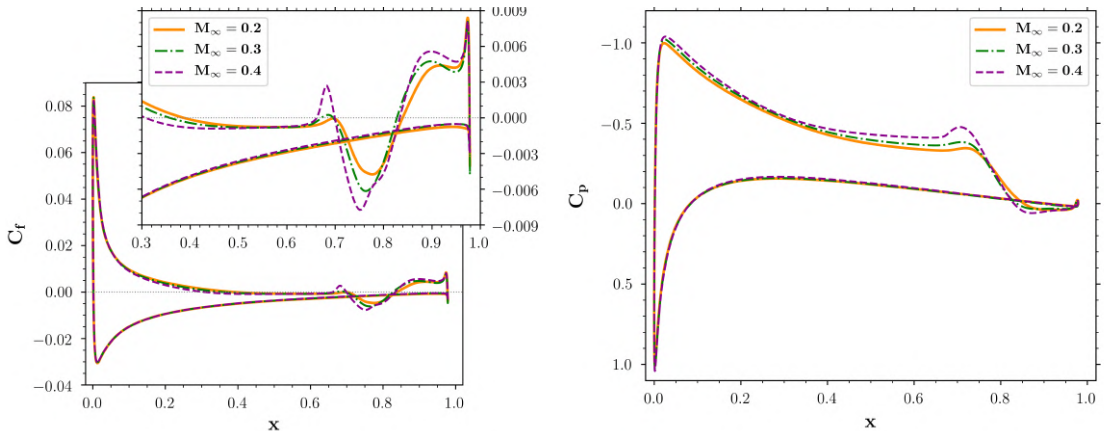

(a) C_f (b) C_P

Figure 10. Surface distribution of skin friction and pressure coefficients.

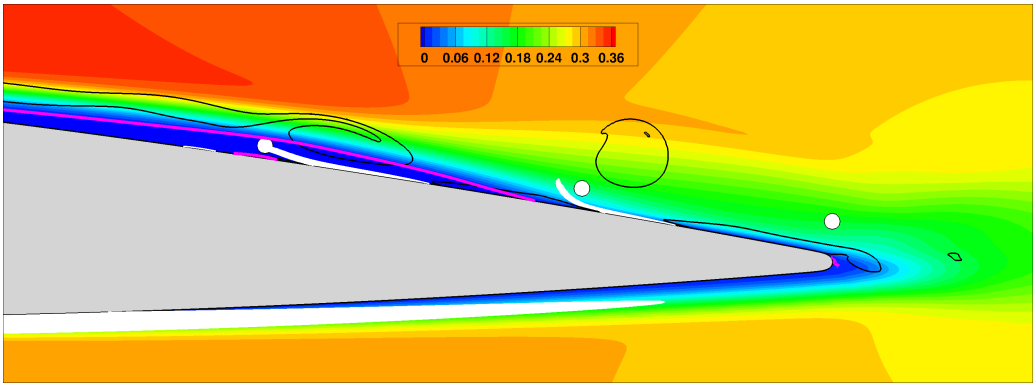

(a) $t = 0.125$

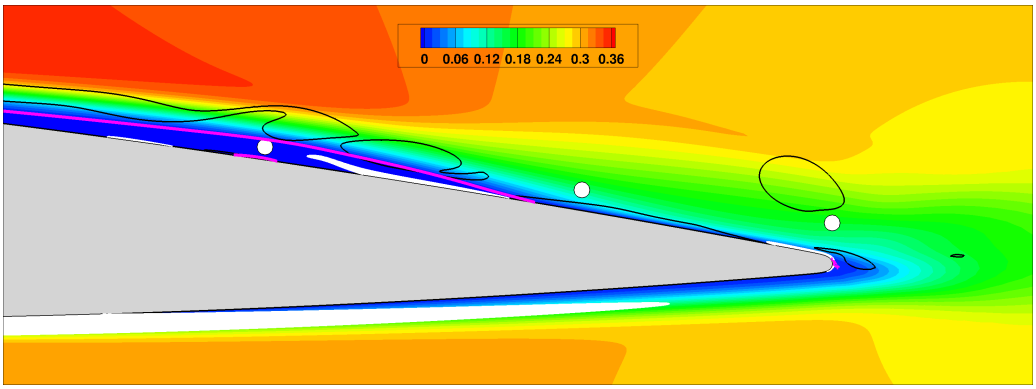

(b) $t = 0.250$

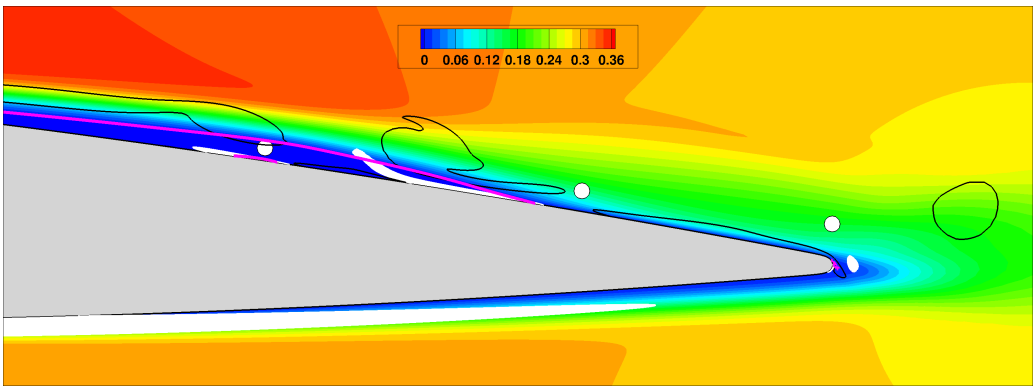

(c) $t = 0.375$

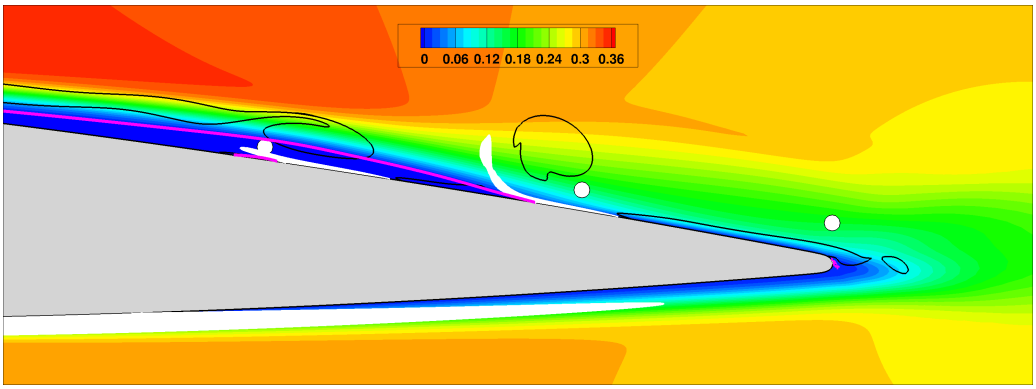

(d) $t = 0.500$

Figure 11. Flow snapshots for different instants showing the vortex dynamics on the airfoil suction side.

4. CONCLUSIONS

In this paper, we perform study of compressibility effects on airfoil secondary tones. A mesh refinement study of an airfoil immersed in a compressible flow at moderate Reynolds number is presented to guarantee that mean and fluctuation flow statistics are converged. Good agreement among all grid solutions is observed and the medium mesh is then used for further investigations of compressibility effects.

The main objective of this work is to perform an assessment of different Mach numbers on the flowfield. It is shown that some flow properties change with Mach number, such as velocity profiles, skin friction and steady pressure. However, it is found that the multiple tones present in the spectral analysis scale with the boundary layer thickness. Hence, for a duet of moderate Reynolds and Mach numbers, the main features of the flow do not seem to change significantly. In other words, the behavior of the spectra, which represent the most important feature investigated here, is maintained with a main tone plus equidistant secondary tones. The tone frequencies are shown to have a scaling based on physical properties of the flow and, hence, more thorough analysis can be performed exclusively for a single Mach number without compromising the investigations. Despite this fact, the frequency and amplitude of the main tone is shown to change depending on the Mach number.

These findings are extremely beneficial when more expensive simulations, such as three-dimensional computations of similar setups are to be performed. In this case, the spectral convergence of the low frequency tones is a computationally expensive task and reducing the number of parameters to study is desirable.

5. ACKNOWLEDGEMENTS

The authors of this work would like to acknowledge Fundação de Amparo à Pesquisa do Estado de São Paulo, FAPESP, for supporting the present work under research grants No. 2013/08293-7, 2018/11835-0 and 2019/20437-0. The authors thank CENAPAD-SP (Project 551) and LNCC-Cluster SDumont (Project SIMTURB) for providing the computer resources used in this study.

6. REFERENCES

Arbey, H. and Bataille, J., 1983. "Noise generated by airfoil profiles placed in a uniform laminar flow". *Journal of Fluid Mechanics*, Vol. 134, pp. 33–47. ISSN 1469-7645. doi:10.1017/S0022112083003201.

Arcondoulis, E.J.G., Doolan, C.J., Zander, A.C. and Brooks, L.A., 2010. "A review of trailing edge noise generated by airfoils at low to moderate Reynolds number". *Acoustics Australia*, Vol. 38, pp. 129–133.

Beam, R. and Warming, R., 1978. "An implicit factored scheme for the compressible Navier-Stokes equations". *AIAA Journal*, Vol. 16, No. 4, pp. 393–402. ISSN 0001-1452. doi:10.2514/3.60901.

Brooks, T.F., Pope, D.S. and Marcolini, M.A., 1989. "Airfoil self-noise and prediction". Technical report, NASA.

Clark, L.T., 1971. "The radiation of sound from an airfoil immersed in a laminar flow". *Journal of Engineering for Gas Turbines and Power*, Vol. 93, No. 4, pp. 366–376. ISSN 0742-4795. doi:10.1115/1.3445595.

de Pando, M.F., Schmid, P.J. and Sipp, D., 2014. "A global analysis of tonal noise in flows around aerofoils". *Journal of Fluid Mechanics*, Vol. 754, pp. 5–38.

Desquesnes, G., Terracol, M. and Sagaut, P., 2007. "Numerical investigation of the tone noise mechanism over laminar airfoils". *Journal of Fluid Mechanics*, Vol. 591, pp. 155–182. ISSN 1469-7645. doi:10.1017/S0022112007007896.

Fink, M.R., 1975. "Prediction of airfoil tone frequencies". *Journal of Aircraft*, Vol. 12, No. 2, pp. 118–120. ISSN 0021-8669. doi:10.2514/3.44421.

Hersh, A. and Hayden, R., 1971. "Aerodynamics sound radiation from lifting surfaces with and without leading edge serrations". Technical report, NASA.

Lele, S.K., 1992. "Compact finite difference schemes with spectral-like resolution". *Journal of Computational Physics*, Vol. 103, No. 1, pp. 16–42. ISSN 0021-9991. doi:http://dx.doi.org/10.1016/0021-9991(92)90324-R.

Longhouse, R., 1977. "Vortex shedding noise of low tip speed, axial flow fans". *Journal of Sound and Vibration*, Vol. 53, No. 1, pp. 25–46. ISSN 0022-460X. doi:http://dx.doi.org/10.1016/0022-460X(77)90092-X.

Massarotti, M.R. and Wolf, W.R., 2018. "Aeroacoustic analysis of automotive roof crossbars through on-track acoustic measurements". *Applied Acoustics*, Vol. 142, pp. 95–105.

Nagarajan, S., Lele, S.K. and Ferziger, J.H., 2003. "A robust high-order compact method for large eddy simulation". *Journal of Computational Physics*, Vol. 191, No. 2, pp. 392–419. ISSN 0021-9991. doi:http://dx.doi.org/10.1016/S0021-9991(03)00322-X.

Paterson, R., Vogt, P., Fink, M. and Munch, C., 1973. "Vortex noise of isolated airfoils". *Journal of Aircraft*, Vol. 10, pp. 296–302.

Pröbsting, S., Serpieri, J. and Scarano, F., 2014. "Experimental investigation of aerofoil tonal noise generation". *Journal of Fluid Mechanics*, Vol. 747, pp. 656–687.

Ricciardi, T.R., Ribeiro, J.H.M. and Wolf, W.R., 2019. "Analysis of coherent structures in large-eddy simulations of a

naca0012 airfoil". In *AIAA Scitech 2019 Forum, AIAA Paper 2019-0320*.

Ricciardi, T.R., Arias-Ramirez, W. and Wolf, W.R., 2020. "On secondary tones arising in trailing-edge noise at moderate reynolds numbers". *European Journal of Mechanics - B/Fluids*, Vol. 79, pp. 54 – 66. ISSN 0997-7546. doi: https://doi.org/10.1016/j.euromechflu.2019.08.015.

Sanjose, M., Towne, A., Jaiswal, P., Moreau, S., Lele, S.K. and Mann, A., 2019. "Modal analysis of the laminar boundary layer instability and tonal noise of an airfoil at Reynolds number 150,000". *International Journal of Aeroacoustics*, Vol. 18, pp. 317–350.

Tam, C.K.W., 1974. "Discrete tones of isolated airfoils". *The Journal of the Acoustical Society of America*, Vol. 55, No. 6, pp. 1173–1177. doi:http://dx.doi.org/10.1121/1.1914682.

Wolf, W.R., Azevedo, J.L.F. and Lele, S.K., 2012a. "Convective effects and the role of quadrupole sources for aerofoil aeroacoustics". *Journal of Fluid Mechanics*, Vol. 708, pp. 502–538. ISSN 1469-7645. doi:10.1017/jfm.2012.327.

Wolf, W.R., Azevedo, J.L.F. and Lele, S.K., 2013. "Effects of mean flow convection, quadrupole sources and vortex shedding on airfoil overall sound pressure level". *Journal of Sound and Vibration*, Vol. 332, pp. 6905–6912.

Wolf, W.R., Lele, S.K., Jothiprasard, G. and Cheung, L., 2012b. "Investigation of noise generated by a DU96 airfoil". In *18th AIAA/CEAS Aeroacoustics Conference (33th AIAA Aeroacoustics Conference)*. pp. 1–15.

7. RESPONSIBILITY NOTICE

The authors are solely responsible for the printed material included in this paper.